International Geology Review, Vol. 46, 2004, p. 332–346.

Upper Paleozoic Basalts in the Southern Yangtze Block: Geochemical and Sr-Nd Isotopic Evidence for Asthenosphere-Lithosphere Interaction and Opening of the Paleo-Tethyan Ocean

FENG GUO,[1] WEI-MING FAN, YUE-JUN WANG, AND CHAO-WEN LI

Key Laboratory of Marginal Sea Geology, Guangzhou Institute of Geochemistry and South China Sea Institute of Oceanology, Chinese Academy of Sciences, Wushan, Guangzhou, 510640 China

Abstract

Basalts in the Youjiang Basin of the southern Yangtze block, south China, consist of Upper Devonian (D_3) tholeiitic volcanics grading to Lower Carboniferous (C_1) alkali basalts. Alkali basalts are generally enriched in incompatible elements relative to tholeiites, having higher Zr, Nb, Hf, Th, LREE, Ti and P abundances, a La/Sm_{CN} range of 2.3–2.8, a La/Yb_{CN} range of 5.9–7.5, a $^{87}Sr/^{86}Sr(i)$ range of 0.7050–0.7053, and $\varepsilon_{Nd}(t)$ values of –1.4 to –0.6. Tholeiites possess a La/Sm_{CN} range of 1.8–2.1, a La/Yb_{CN} range of 3.3–4.6, a $^{87}Sr/^{86}Sr(i)$ range of 0.7047–0.7054, and ε_{Nd} (t) values of –3.1 to –2.2. Both basaltic suites have EM1-like Sr-Nd isotopic signatures; however, their distinctly different La/Nb, Zr/Nb, and Th/Nb values suggest heterogeneous mantle sources. Higher La/Nb (1.03–1.31), Th/Nb (0.22–0.24) and Zr/Nb (8.2–8.5) ratios in the D_3 tholeiites indicate the importance of enriched lithospheric mantle in the petrogenesis, whereas strong OIB-type trace element signatures—e.g., low La/Nb (0.74–0.87), Th/Nb (0.14–0.15) and Zr/Nb (5.3–5.9)—in the C_1 volcanics necessitates an important contribution of an OIB-type asthenosphere. Increasing $\varepsilon_{Nd}(t)$ and La/Sm values coupled with decreasing La/Nb ratios grading from D_3 to C_1 basalts suggest that the D_3 tholeiites were produced at relatively larger melting degrees with higher proportions of enriched components, and that the C_1 alkali basalts were generated at smaller melting degrees with lower proportions of enriched components. Such trends reflect a continuous lithospheric thinning event attending asthenosphere-lithosphere interaction. Progressive rifting episodes explain the petrogenesis of these Upper Paleozoic basalts, suggesting that the southern Yangtze block had become a passive continental margin following the opening and spreading of the Paleo-Tethyan Ocean.

Introduction

THE ULTIMATE SOURCE and reason(s) why volcanism in continental margins occurs remain subjects of considerable debate, despite common links with either lithospheric extension and rifting caused by oceanic opening or subduction of oceanic slabs (e.g., Grove and Kinzler, 1986; Basu et al., 1991; Arculus, 1994; Chung et al., 1994; Hunter and Blake, 1995). In active continental margins, subduction of oceanic slabs introduces H_2O and other volatiles that lower solidus temperatures of peridotites; the produced melts are characterized by island-arc trace-element signatures, i.e., significant large-ion lithophile element (LILE) and light-rare-earth element (LREE) enrichments relative to high-field-strength elements (HFSE) (e.g., Grove and Kinzler, 1986; Davis and Stevenson, 1992; Arculus, 1994; Hunter and Blake, 1995). However, magma generation in passive margins generally is accounted for by asthenospheric upwelling and lithospheric extension; the basaltic melts usually show the affinities of intraplate basalts, i.e., OIB-like trace-element geochemistry (e.g., Smedley, 1986; McKenzie and Bickle, 1988; Basu et al., 1991; Chung et al., 1994; Laflèche et al., 1998; Gorring et al., 2003). Such geochemical differences between basaltic magmas formed along different types of continental margins provide a potential way to elucidate the development history of continental crust.

Following the opening and spreading of the Paleo-Tethyan Ocean, the southern Yangtze block became a continental margin beginning in at least Middle Devonian time (Chen et al., 1994, 2000; Cheng, 1994; Zhang et al., 1985, 1988; Jian et al., 1998; Ren et al., 1999). Whether it was an active or

[1]Corresponding author; email: guofengt@263.net

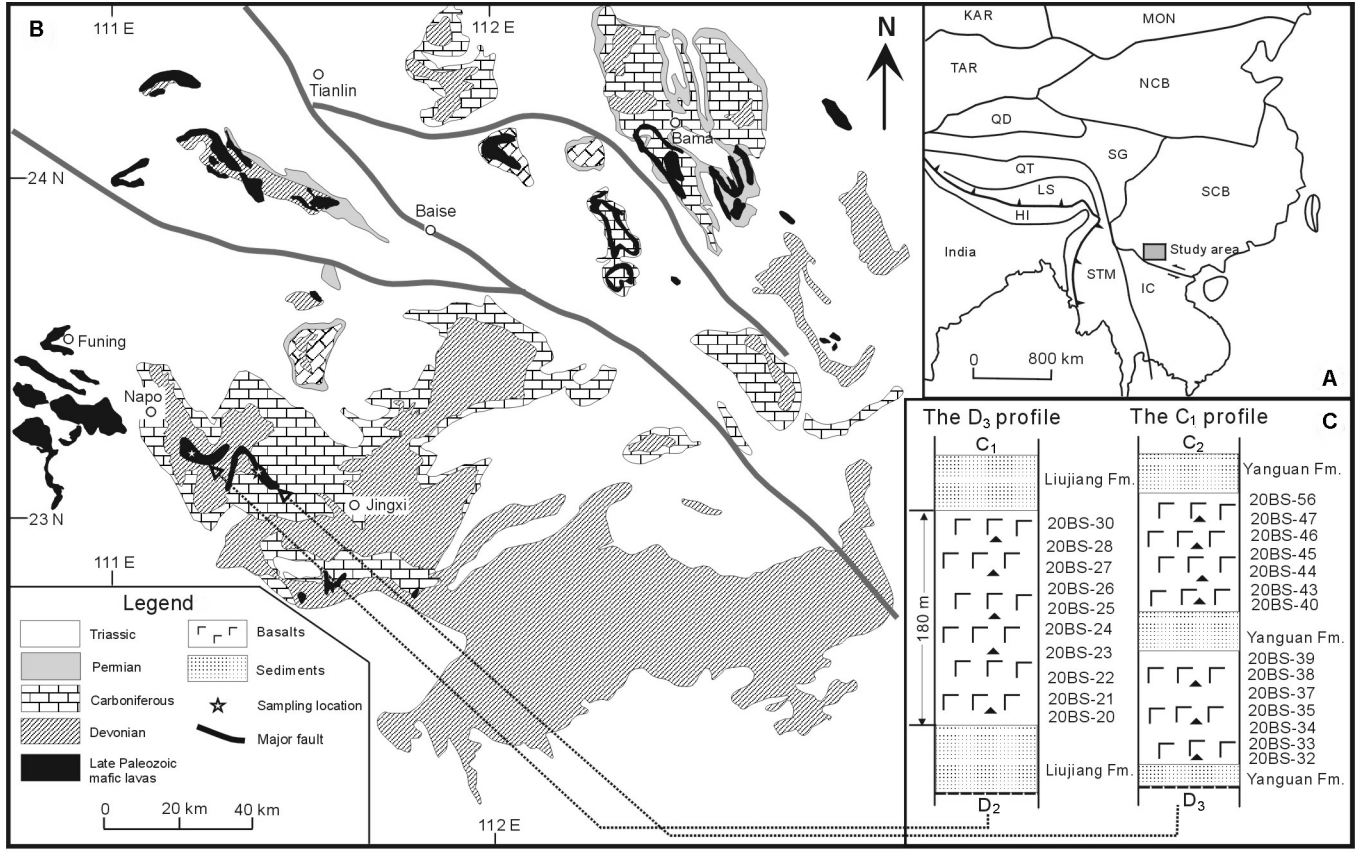

FIG. 1. Distribution of Upper Paleozoic basaltic rocks in Youjiang Basin of the southern Yangtze block (modified after GXBGMR, 1985; Ren et al., 1999) and sampling profiles of the studied D_3 and C_1 basalts. Major terranes of the East Asia continent refer to those of Ren et al. (1999). Abbreviations: SCB = South China block; SG = Songpan-Ganze accretionary complex; QT = Qitang; STM = Shan-Tai-Malay; IC = Indochina; HI = Himalaya; LS = Lhasa; QD = Qaidam; TAR = Tarim; KAR = Karakorum; MON = Mongolia; NCB = North China block.

a passive margin is still poorly constrained although sedimentary records and infilling sequences in the Youjiang Basin suggested that basin formation was initiated under an intracontinental extensional regime (Chen et al., 1994, 2000; Qin et al., 2000). During basin development, Upper Paleozoic basaltic lavas were erupted (GXBGMR, 1985; Wang et al., 1997), providing a rare opportunity for studying the effect of the Paleo-Tethyan Ocean on the geotectonic evolution of the southern Yangtze block. Here we report major-, trace-element, and Sr-Nd isotope data of two basaltic suites erupted in Late Devonian (D_3) and Early Carboniferous (C_1), respectively, in the Youjiang Basin. The objectives of this study are to: (1) characterize the mantle sources beneath the southern Yangtze block; and (2) understand the origins of Upper Paleozoic basalts and their relationship to tectonic evolution of the Paleo-Tethyan Ocean.

Geological Background and Petrography

The South China block (SCB) consists of the Yangtze and Cathaysian blocks, which collided during an early stage of the Neoproterozoic (Li, 1999). Subsequent Neoproterozoic break-up of the Rodinia supercontinent separated the Yangtze from the Cathaysian landmass by the Nanhua rift (Li et al., 1995, 1999; Gilder et al., 1996; Li, 1999; Li and Powell, 2001; Li et al., 2002). This rift was ultimately closed by the end of the Early Paleozoic (e.g., Cheng, 1994; Ren et al., 1999). The Youjiang Basin is located in the southern Yangtze block (Fig. 1A), where Upper Paleozoic pelagic sediments and neritic carbonates thousands of meters thick were deposited. During basin development, scattered basaltic lavas were erupted along its axis and flanks (Fig. 1). Field work and previous geological surveys indicated that eruption of volcanic sequences spanned a prolonged period from Late Devonian to Early Triassic time (Fig. 1B).

Samples studied here were collected in the Jinxi-Napo area (Fig. 1B), where the basaltic lavas are crop out as lenses and interbeddings, well confined by the syn-depositional rocks. The Upper Devonian (D_3) volcanic sequences have a range of 80–180 m thickness, enclosed by lens-shaped limestones of the Upper Devonian Liujiang Formation. They are composed mainly of olivine basalts and basaltic andesites (GXBGMR, 1985), with aphanitic to weakly porphyritic fabrics. The main phenocrysts include olivine and clinopyroxene 1–3 mm in size. Some high-MgO samples (e.g., 20BS-20, 21, and 22) exhibit zones of olivine cumulate enrichment. The matrix comprises mainly fine-grained or aphanitic olivine, clinopyroxene, and plagioclase (<0.2 mm grain sizes) and accessory minerals such as magnetite, ilmenite, and apatite. The Lower Carboniferous (C_1) basaltic lavas, mainly lens-shaped flows, mafic brecciated lavas, and minor tuffs, also occur as parallel to subparallel layers interbedded with limestones and silcalites of the Lower Carboniferous Yanguan Formation (GXBGMR, 1985; Wang et al., 1997). The basalts are generally aphanitic with rare clinopyroxene and plagioclase phenocrysts. Detailed sampling profiles for both basaltic suites and their contact relationship with the sedimentary rocks are shown in Figure 1C.

Analytical Techniques

All samples were crushed to mm scale after removal of weathered rims and handpicked under a magnifier. Fresh chips were selected and washed in an ultrasonic bath before being crushed to <20 mesh in a WC jaw crusher. A split was ground to <160 mesh grain size in an agate ring mill, and this material was used for major- and trace-element analysis. Major elements were performed at Hubei Institute of Geology and Mineral Resource, Ministry of Land and Resources (MLR), by wavelength X-ray fluorescence spectrometry (XRF). The analytical errors for major oxides are less than 2%. FeO was analyzed by wet chemical method. All trace-element concentrations were determined by ICP-MS at Guiyang Institute of Geochemistry, Chinese Academy of Sciences (CAS). Detailed descriptions of the analytical techniques were reported in Qi et al. (2000). Reproducibility is better than 95%, with analytical error less than 5% for most of the analyzed elements, and about 10% for Cr and Ni.

Sr and Nd isotopic ratios were measured at the Institute of Geology and Geophysics, CAS. Rock chips <20 meshes were used for Sr and Nd isotope analyses. Before being ground to <160 mesh and chemical dissolution, these chips were leached by purified 6N HCl for 24 hours at room temperature to avoid the influence of alteration or weathering, especially for Sr isotopic ratios. Sr and Nd isotopic ratios were normalized to $^{86}Sr/^{88}Sr = 0.1194$ and $^{146}Nd/^{144}Nd = 0.7219$, respectively. The La Jolla standard yielded $^{143}Nd/^{144}Nd = 0.511862\pm12$ (n=10) and the NBS987 standard gave $^{87}Sr/^{86}Sr = 0.710240 \pm 10$ ($n = 6$). The whole procedure blank

TABLE 1. Major- and Trace-Element Contents of Upper Devonian Basaltic Lavas in Youjiang Basin, Southern Yangtze Block

Sample:	20BS-20	20BS-21	20BS-22	20BS-23	20BS-24	20BS-25	20BS-26	20BS-27	20BS-28	20BS-30
Rock type:[1]	Ol-Bas	Ol-Bas	Ol-Bas	Bas	Bas-And	Bas	Bas-And	Bas-And	Bas	Bas
SiO_2	45.41	46.15	45.81	48.56	51.47	50.95	51.78	52.15	49.88	48.74
TiO_2	0.72	0.8	0.79	1.06	1.27	1.25	1.3	1.34	1.25	0.98
Al_2O_3	10.51	12.28	11.72	14.77	15.17	15.53	15.24	15.69	15.49	11.77
Fe_2O_3	1.36	1.85	1.55	1.66	1.83	1.5	2.65	1.64	2.21	1
FeO	10.6	9.3	10	8.58	7.38	8.17	6.57	7.13	7.5	9.83
CaO	5.85	5.51	5.66	6.34	8.87	6.36	8.4	7.44	8.92	6.59
MgO	17.04	14.06	15.08	9.15	5.72	6.42	5.67	5.57	6.26	12.28
MnO	0.16	0.15	0.16	0.14	0.13	0.11	0.11	0.11	0.13	0.16
K_2O	0.49	1.41	0.62	2.07	0.77	2.66	1.25	0.92	0.99	0.92
Na_2O	1.73	2.07	2.17	2.83	2.73	2.67	2.96	3.29	2.3	2.64
P_2O_5	0.11	0.12	0.12	0.16	0.18	0.19	0.19	0.2	0.18	0.14
H_2O	5.78	5.88	5.96	4.37	4.22	3.92	3.59	4.24	4.68	4.66
CO_2	0.01	0.11	0.11	0.06	0.06	0.06	0.06	0.06	0.01	0.06
Total	99.77	99.69	99.75	99.75	99.8	99.79	99.77	99.78	99.8	99.77
Cr	761	632	650	384	220	219	209	192	273	491
Ni	460	323	407	180	55	73	62	64	80	281
Rb	19.69	18.91	14.17	42.78	14.72	46.42	20.77	15.36	20.76	18.68
Sr	186	236	143	320	357	314	496	271	311	186
Y	10.51	17.27	15.81	19.82	30.86	21.60	24.59	23.07	21.58	25.89
Zr	50.4	56.8	56.5	76.0	95.4	97.5	97.8	104.5	92.2	73.6
Nb	6.15	6.77	6.79	9.07	11.41	11.84	11.81	12.80	10.80	8.99
Ba	120	217	327	350	138	474	256	173	147	179
Hf	1.65	1.87	1.78	2.39	3.06	3.10	3.07	3.19	2.92	2.40
Ta	0.36	0.41	0.39	0.58	0.64	0.73	0.72	0.79	0.64	0.54
Th	1.38	1.52	1.58	2.14	2.56	2.67	2.75	3.00	2.57	2.01
U	0.24	0.28	0.31	0.39	0.48	0.53	0.48	0.54	0.46	0.36
La	7.03	7.94	8.59	10.16	14.90	13.07	12.17	14.09	12.41	10.21
Ce	13.82	16.25	18.32	21.59	31.02	28.26	26.82	29.61	26.95	21.03
Pr	1.70	1.98	2.18	2.53	3.59	3.30	3.30	3.60	3.30	2.69
Nd	8.12	9.38	10.00	11.62	15.72	15.03	14.67	16.03	14.38	11.63
Sm	2.08	2.73	2.84	3.18	4.43	4.01	4.02	4.16	4.02	3.27
Eu	0.60	0.77	0.92	1.19	1.33	1.09	1.22	1.31	1.27	1.00
Gd	2.20	3.14	3.16	3.70	5.32	4.25	4.23	4.64	4.34	4.20
Tb	0.35	0.50	0.51	0.58	0.85	0.72	0.73	0.79	0.75	0.71
Dy	2.22	2.76	3.16	3.53	5.05	4.29	4.39	4.67	4.13	4.45
Ho	0.43	0.60	0.59	0.72	1.07	0.83	0.85	0.87	0.84	0.89
Er	1.19	1.61	1.60	1.87	2.84	2.29	2.22	2.37	2.23	2.48
Tm	0.19	0.21	0.22	0.22	0.39	0.30	0.34	0.32	0.30	0.32
Yb	1.07	1.36	1.42	1.53	2.39	2.02	1.96	2.12	1.83	2.11
Lu	0.15	0.18	0.21	0.24	0.34	0.28	0.28	0.34	0.26	0.30
La/Sm_{CN}	2.1	1.8	1.9	2.0	2.1	2.1	1.9	2.1	1.9	2.0
La/Yb_{CN}	4.4	3.9	4.1	4.5	4.2	4.4	4.2	4.5	4.6	3.3
La/Nb	1.14	1.17	1.26	1.12	1.31	1.10	1.03	1.10	1.15	1.13
Th/Nb	0.23	0.23	0.23	0.24	0.22	0.23	0.23	0.23	0.24	0.22
Zr/Nb	8.2	8.4	8.3	8.4	8.4	8.2	8.3	8.2	8.5	8.2

[1]Ol-bas = olivine basalt; Bas = basalt; Bas-And = basaltic andesite.

TABLE 2. Major- and Trace-Element Contents of Lower Carboniferous Basalts in Youjiang Basin, Southern Yangtze Block

Sample:	20BS-32	20BS-33	20BS-34	20BS-35	20BS-37	20BS-38	20BS-39	20BS-40	20BS-43	20BS-44	20BS-45	20BS-46	20BS-47	20BS-56
Rock type:	Bas	Bas	Bas	Bas	Bas	Bas	Ol-Bas	Bas-And	Bas	Bas	Bas	Bas	Bas	Bas-And
SiO_2	49.99	50.23	49.22	49.23	50.43	49.44	48.19	54.47	49.73	47.91	46.77	47.39	45.51	51.36
TiO_2	1.43	1.42	1.44	1.49	1.42	1.39	1.52	1.32	1.47	1.46	1.43	1.45	1.48	1.56
Al_2O_3	14.08	13.64	14.15	14.12	13.51	13.5	14.02	13.12	14.00	14.17	13.24	13.82	13.65	13.67
Fe_2O_3	1.49	1.12	0.98	1.07	0.91	0.96	1.56	3.74	1.04	1.39	1.59	1.44	1.5	7.28
FeO	7.97	8.43	8.87	9.03	8.23	8.17	8.20	6.07	8.70	8.33	8.83	9.53	9.68	3.67
CaO	6.88	8.75	7.69	7.85	7.81	8.83	6.46	4.74	6.98	7.69	10.8	9.14	9.35	5.57
MgO	7.85	7.60	8.62	7.95	8.51	8.34	10.18	7.31	7.91	7.83	7.15	7.52	8.06	6.98
MnO	0.11	0.12	0.13	0.13	0.13	0.14	0.15	0.10	0.12	0.12	0.16	0.13	0.14	0.1
K_2O	0.73	0.31	0.73	0.30	0.19	0.69	1.13	0.81	0.68	0.92	0.76	1.01	1.64	2.45
Na_2O	4.49	4.12	3.32	4.19	4.32	3.02	2.97	4.35	4.3	3.77	3.22	3.12	2.32	3.44
P_2O_5	0.26	0.26	0.28	0.27	0.27	0.26	0.28	0.26	0.28	0.27	0.26	0.27	0.27	0.29
H_2O	3.85	3.36	4.06	3.88	3.89	4.23	4.99	3.40	3.81	4.21	3.76	3.97	4.3	2.88
CO_2	0.66	0.44	0.28	0.28	0.17	0.83	0.11	0.11	0.77	1.71	1.82	0.99	1.87	0.5
Total	99.79	99.8	99.77	99.79	99.79	99.8	99.76	99.80	99.79	99.78	99.79	99.78	99.77	99.75
Cr	274	276	251	287	267	270	197	243	290	263	243	283	314	340
Ni	209	183	130	215	173	208	84	139	212	158	144	207	237	195
Rb	8.74	2.96	6.92	3.00	1.66	8.77	14.45	9.01	5.85	10.89	6.73	14.71	26.96	35.34
Sr	308	276	282	314	291	346	318	301	266	306	369	383	257	406
Y	19.87	20.55	19.80	20.03	20.51	19.27	20.56	19.13	18.52	18.62	19.01	21.24	19.47	24.24
Zr	115.0	115.9	114.0	121.2	115.8	113.4	126.6	110.2	116.7	121.5	114.6	124.5	121.0	121.4
Nb	20.69	20.84	20.78	21.66	22.01	20.67	23.08	20.15	21.39	22.30	21.40	22.65	22.97	20.74
Ba	160	62	207	89	56	201	338	214	520	133	187	290	140	+132

Sample	20BS-32	20BS-33	20BS-34	20BS-35	20BS-37	20BS-38	20BS-39	20BS-40	20BS-43	20BS-44	20BS-45	20BS-46	20BS-47	20BS-56
Hf	3.44	3.34	3.26	3.59	3.55	3.37	3.67	3.17	3.55	3.33	3.70	3.41	3.55	3.38
Ta	1.25	1.22	1.21	1.32	1.21	1.27	1.36	1.11	1.15	1.31	1.29	1.25	1.28	1.33
Th	3.19	2.93	2.87	3.08	3.11	3.07	3.45	2.89	3.16	3.12	3.12	3.02	3.35	3.18
U	0.70	0.65	0.59	0.68	0.66	0.68	0.77	0.65	0.79	0.74	0.73	0.65	0.74	0.75
La	17.19	16.37	15.55	17.07	16.64	17.80	18.25	17.54	17.90	15.90	17.16	16.08	18.62	18.76
Ce	35.63	34.10	32.18	33.96	33.51	35.87	37.44	35.80	35.28	33.28	34.00	33.57	38.01	36.93
Pr	4.13	3.99	3.84	3.92	3.97	4.10	4.37	4.22	4.34	3.93	4.18	3.88	4.36	4.22
Nd	17.35	17.62	15.88	17.70	17.30	17.42	18.19	17.13	18.65	16.87	17.21	17.14	18.67	17.96
Sm	4.24	4.51	3.97	4.50	4.10	4.12	4.68	4.17	4.79	4.04	4.51	4.05	4.34	4.26
Eu	0.98	1.21	1.09	1.13	1.10	1.31	1.50	1.13	1.42	1.15	1.36	1.30	1.24	1.39
Gd	4.37	4.14	4.02	4.40	4.13	4.12	4.81	4.40	4.79	3.93	4.19	4.29	4.49	4.48
Tb	0.64	0.73	0.65	0.65	0.69	0.66	0.71	0.62	0.79	0.61	0.63	0.70	0.72	0.68
Dy	3.97	3.92	3.84	3.88	3.94	3.87	3.90	3.81	4.58	3.78	3.63	3.90	3.99	3.86
Ho	0.73	0.72	0.70	0.75	0.79	0.72	0.78	0.68	0.83	0.68	0.72	0.70	0.77	0.73
Er	2.03	2.05	1.95	2.00	2.16	1.88	2.07	1.89	2.33	1.86	1.85	1.97	2.07	2.10
Tm	0.27	0.27	0.26	0.25	0.28	0.28	0.28	0.26	0.30	0.26	0.28	0.29	0.30	0.28
Yb	1.90	1.67	1.58	1.71	1.90	1.64	1.80	1.58	2.03	1.62	1.71	1.72	1.82	1.71
Lu	0.24	0.26	0.25	0.24	0.27	0.21	0.25	0.22	0.28	0.20	0.24	0.24	0.27	0.24
La/Sm_{CN}	2.6	2.3	2.5	2.4	2.6	2.7	2.5	2.7	2.5	2.4	2.5	2.7	2.8	2.4
La/Yb_{CN}	6.1	6.6	6.7	6.8	5.9	7.4	6.8	7.5	6.6	6.8	6.3	6.9	7.4	6.0
La/Nb	0.83	0.79	0.75	0.79	0.76	0.86	0.79	0.87	0.74	0.77	0.75	0.82	0.82	0.86
Th/Nb	0.15	0.14	0.14	0.14	0.14	0.15	0.15	0.14	0.15	0.14	0.14	0.15	0.14	0.15
Zr/Nb	5.6	5.6	5.5	5.6	5.3	5.5	5.5	5.5	5.5	5.4	5.4	5.5	5.3	5.9

[1]Ol-bas = olivine basalt; Bas = basalt; Bas-And = basaltic andesite.

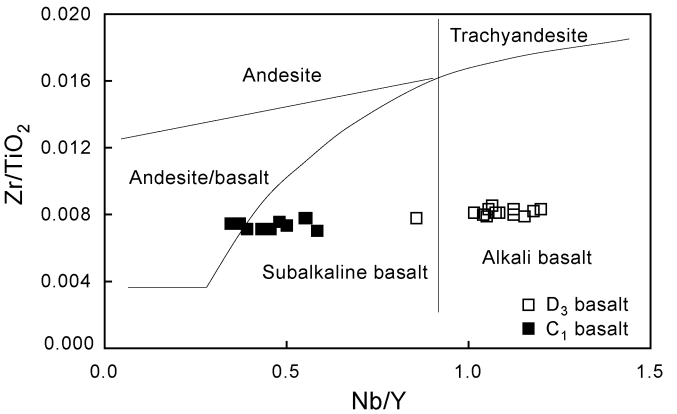

FIG. 2. Zr/TiO_2 vs. Nb/Y classification diagram for the Youjiang Basin basalts (modified after Floyd and Winchester, 1978).

ranges from 2 to 5×10^{-10}g for Sr, and less than 5×10^{-11}g for Nd. Analytical errors for Sr and Nd isotopic ratios are given as 2σ. The major- and trace-element compositions and Sr-Nd isotope data of Upper Paleozoic basalts in the Youjiang Basin are listed respectively in Tables 1, 2, and 3.

Results

Alteration

All rocks sampled for this study experienced various degrees of alteration, as reflected by high loss on ignition (LOI = 3.38–6.17%; Tables 1 and 2). During low-temperature hydrothermal alteration, the abundances of mobile elements like K, Na, Cs, Rb, Ba, and U may be affected, so these elements are avoided in the petrogenetic modeling. The following discussion will mainly focus on the behavior of relatively immobile elements such as REE, HFSE, Th, transition metals (e.g., Cr, Ni), and Sr-Nd isotopic data. It is necessary to point out that the age-corrected Sr isotopic ratios might also be affected by Rb and Sr abundances obtained by ICP-MS analysis, but this would not influence the petrogenetic discussion very much because all analyzed samples still have relatively low $^{87}Rb/^{86}Sr$ and slightly variable $^{87}Sr/^{86}Sr$ ratios (Table 3).

Major and trace elements

On a volatile-free basis, the Youjiang Basin volcanic rocks have a SiO_2 range of 48.32–56.57% and a MgO range of 5.83–18.13%, and all samples are basaltic in composition. Variations in major and trace element concentrations are ascribed both to alteration and to an inherent compositional variation of the basalts, which range from subalkalic (tholeiitic, 10 samples, Table 1) to alkalic basalts (14 samples, Table 2) on the Zr/TiO_2 vs. Nb/Y discrimination diagram (Fig. 2). This subdivision is used to facilitate the presentation of data, but both basaltic suites are compositionally heterogeneous, and intergradational.

The alkali basalts are generally enriched in incompatible elements relative to the tholeiites, having higher abundances in Zr, Nb, Hf, Th, LREE, Ti, and P (Tables 1 and 2 and Fig. 3). Correlation between MgO and other elements is obvious in the tholeiites, e.g., positive correlation of MgO versus Cr, Ni, and negative correlation versus Al_2O_3, CaO, TiO_2, Nb, Zr, and Sr, suggesting an important role of olivine fractionation (Fig. 3). The alkali basalts show a weak correlation between MgO and other elements (Fig. 3), indicative of a less important role or fractional crystallization during magma evolution.

Both basaltic suites display similar chondrite-normalized REE patterns (Fig. 4). The alkali basalts show stronger REE fractionation than that of tholeiites, possessing a La/Yb_{CN} range of 5.9–7.5, and a La/Sm_{CN} range of 2.3–2.8; the tholeiites have a La/Yb_{CN} range of 3.3–4.6, and a La/Sm_{CN} range of 1.8–2.1. In the primitive mantle–normalized multi-element diagrams (Fig. 5), the Youjiang Basin basalts generally exhibit OIB-like trace-element signatures except for variably positive Th anomalies. Despite the compositional ranges, both basaltic suites have

constant Th/Nb and Zr/Nb values (Th/Nb = 0.22–0.24 and Zr/Nb = 8.2–8.5 in D_3 tholeiites, Table 1; Th/Nb = 0.14–0.15 and Zr/Nb = 5.3–5.8 in C_1 alkali basalts, Table 2).

Sr-Nd isotope data

Measured and age-corrected Sr and Nd isotope data are listed in Table 3. Both basaltic suites have slightly variable Sr and Nd isotope data. The tholeiites span a $^{87}Sr/^{86}Sr$ range of 0.705643–0.706517 and $^{143}Nd/^{144}Nd$ range of 0.512416 – 0.512450, as well as an initial $^{87}Sr/^{86}Sr(i)$ range of 0.70480–0.70539 and a $\varepsilon_{Nd}(t)$ range of –3.1 to –2.2. The alkali basalts span a $^{87}Sr/^{86}Sr$ range of 0.705365–0.706454 and $^{143}Nd/^{144}Nd$ of 0.512454–0.512490, as well as an initial $^{87}Sr/^{86}Sr(i)$ range of 0.70499–0.70528 and a $\varepsilon_{Nd}(t)$ range of –1.4 to –0.6. Both basalt suites plot within the range of the EM1-type oceanic-island basalts (OIB) in a $^{87}Sr/^{86}Sr(i)$ vs. $\varepsilon_{Nd}(t)$ diagram (Fig. 6), different from Upper Permian Emeishan flood basalts in southwestern China (e.g., Chung and Jahn, 1995; Xu et al., 2001).

Discussion

As a whole, Upper Paleozoic Youjiang Basin basaltic lavas in the southern Yangtze block have OIB-like elemental geochemistry and EM1-type Sr-Nd isotope data. To account for their enriched characters (especially in Sr-Nd isotopes, REE and Th), petrogenesis of both tholeiitic and alkalic basalts necessitates the involvement of: (1) an enriched component, either asthenospheric (e.g., a deep mantle plume) or lithospheric in origin; or (2) enrichment processes, such lower degrees of melting, crustal contamination, and/or high degrees of fractional crystallization. In the following discussion, we will address in turn the following issues: (1) role of petrogenetic process *en route* to the surface; (2) source characteristics; and (3) magma genesis of the Youjiang Basin basalts and the relationship with the tectonic evolution of the Paleo-Tethyan Ocean.

Effect of crustal contamination

Basalts erupted in continental settings are characteristically enriched in trace-element and isotopic features relative to oceanic counterparts. The debate continues as to the importance of processes operating at crustal levels; thus it is necessary to evaluate the possible effects of crustal contamination during passage through the lithosphere. As can be seen in Table 3, both basaltic suites have slight variation in

TABLE 3. Sr and Nd Isotope Analysis of Upper Paleozoic Basalts in the Youjiang Basin, Southern Yangtze Block[1]

Sample:	Rb, ppm	Sr, ppm	$^{87}Rb/^{86}Sr$	$^{87}Sr/^{86}Sr \pm 2\sigma$	$^{87}Sr/^{86}Sr(i)$	Sm, ppm	Nd, ppm	$^{147}Sm/^{144}Nd$	$^{143}Nd/^{144}Nd \pm 2\sigma$	$\varepsilon_{Nd}(t)$
20BS-20	19.69	186	0.3067	0.706517±20	0.70492	2.08	8.12	0.1553	0.512421±12	–2.30
20BS-24	14.72	357	0.1197	0.705643±28	0.70502	4.43	15.72	0.1703	0.512450±12	–2.44
20BS-26	20.77	496	0.1214	0.706019±14	0.70539	4.02	14.67	0.1656	0.512449±7	–2.24
20BS-28	20.76	311	0.1937	0.706088±20	0.70508	4.02	14.38	0.1690	0.512428±8	–2.81
20BS-30	18.68	186	0.2917	0.706316±20	0.70480	3.27	11.63	0.1699	0.512416±8	–3.08
20BS-32	8.74	308	0.0823	0.705647±18	0.70525	4.24	17.35	0.1477	0.512466±8	–1.23
20BS-38	8.77	346	0.0735	0.705365±17	0.70501	4.12	17.42	0.1430	0.512473±13	–0.89
20BS-40	9.01	301	0.0868	0.705411±15	0.70499	4.17	17.13	0.1471	0.512454±9	–1.44
20BS-45	6.73	369	0.0528	0.705540±19	0.70528	4.05	17.14	0.1428	0.512490±9	–0.55
20BS-56	35.34	406	0.2525	0.706454±21	0.70523	4.79	18.65	0.1552	0.512473±10	–1.42

[1]Sm, Nd, Rb, and Sr abundances are measured by ICP-MS method. The initial Sr and Nd isotope data are respectively corrected at 365 Ma and 340 Ma for D_3 and C_1 samples.

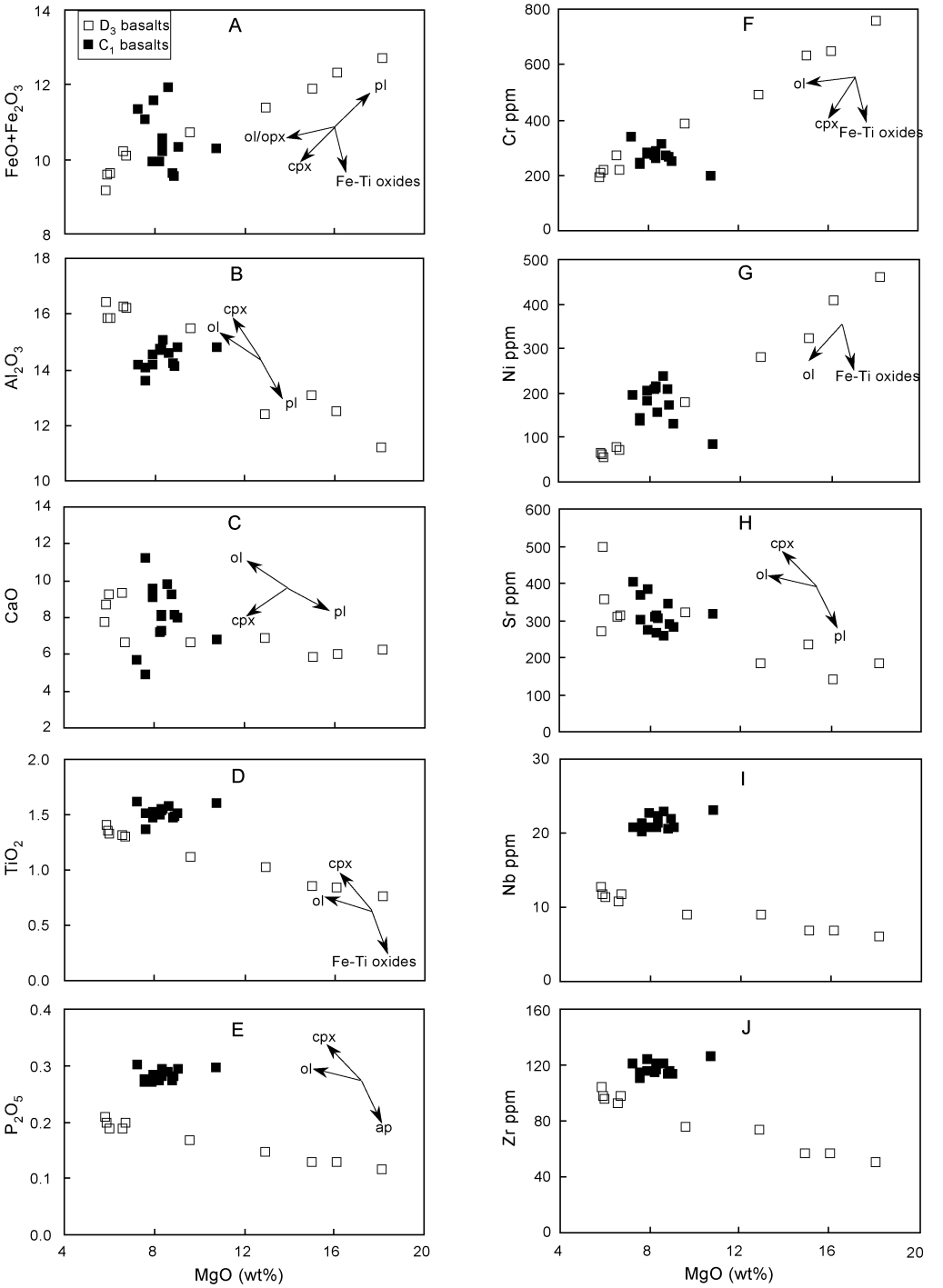

FIG. 3. MgO vs. other element diagrams of Upper Paleozoic basaltic lavas in the Youjiang Basin. The major oxide contents are loss-free normalized to 100%. Abbreviations: ol = olivine; cpx = clinopyroxene; pl = plagioclase; ap = apatite.

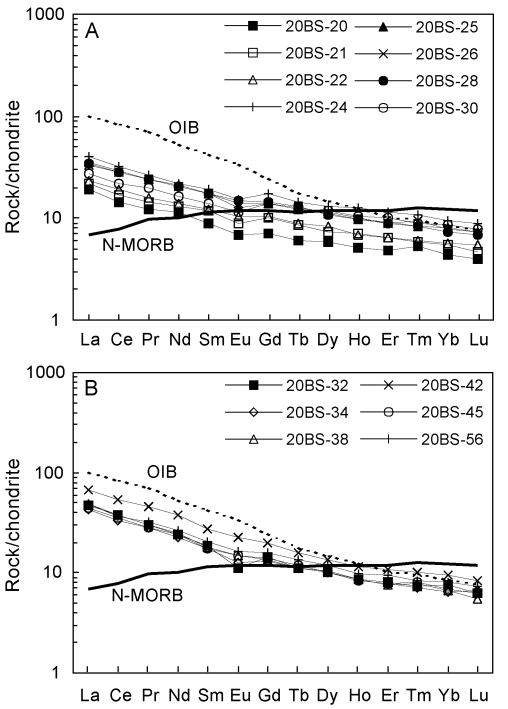

FIG. 4. Chondrite-normalized REE patterns of Upper Paleozoic basaltic lavas in the Youjiang Basin. The subparallel REE patterns in the D_3 tholeiites suggest an important role for FC process during magma evolution, consistent with the variation trend of Figure 3. Chondrite values (in ppm) are from Taylor and McLennan (1985); and N-MORB, and OIB are from Sun and McDonough (1989).

Nd isotope data, with a range of $\varepsilon_{Nd}(t)$ values of less than 1 unit, precluding significant effects of crustal contamination on magma evolution. If crustal contamination had occurred, the slightly variable Th/Nb and Zr/Nb, and moderately enriched Sr isotope data in both suites would have favored contamination by lower continental crust (LCC) instead of upper continental crust (UCC) (Fig. 7A).

Case studies of basaltic magmas contaminated by lower crust are rarely presented (e.g., Peng et al., 1994). In such cases, decreasing density contrast between the mafic lower crust and the upper mantle makes the Moho an ideal place for magma to accumulate. Advanced fractional crystallization together with heat input from an ascending plume may support assimilation of lower-crustal rocks (e.g., Jung and Hoernes, 2000). This requires a high geotherm and a high-pressure fractional assemblage to make lower crust a potential assimilator. However, the fact that both basaltic suites in the Youjiang Basin have low Al_2O_3 (<16%) contents favored low-pressure fractionation (e.g., Laflèche et al., 1998). Additionally, the scattered exposure of Upper Paleozoic basaltic lavas also precludes the possibility of the presence of an ascending plume (see following discussion).

On the other hand, geochemical considerations also rule out the possibility of significant lower-crustal contamination. Despite considerable debate concerning the composition and lithology of the LCC (e.g., Rudnick and Fountain, 1995), a general LCC feature estimated in previous studies suggests that it has high Zr/Nb and La/Nb ratios (Zr/Nb = 11.7 and La/Nb = 1.83, e.g., Taylor and McLennan, 1985; Zr/Nb = 13.6, La/Nb = 1.6, e.g., Rudnick and Fountain, 1995). If lower crust contamination had occurred, both Zr/Nb and La/Nb would have been increased in the evolved magmas. But this is not observed in the La/Nb vs. Zr/Nb diagram (Fig. 7B), in which both basaltic suites show slightly varied Zr/Nb values following an increase in La/Nb. Therefore, the effect of crust contamination on magmatic evolution is negligible, and the geochemical and Sr-Nd isotopic variations in both basaltic suites were probably inherited from heterogeneous sources.

Source characteristics

Generation of continental basalts with OIB-like trace-element geochemistry is frequently considered as a consequence of mantle plume activity (e.g., Weaver, 1991). Mixing of enriched and depleted components in a deep mantle plume is commonly employed to account for variable enrichment in incompatible trace elements. In contrast with the Upper Permian Emeishan large igneous provinces in southwestern China (e.g., Chung and Jahn, 1995; Xu et al., 2001), scattered exposure of volcanic rocks in the Youjiang Basin likely resulted from continental extension. A plume hypothesis is further denied by the lack of a contemporaneous plume track and evidence for regional doming on adjacent continental blocks (Griffiths and Campbell, 1991; Laflèche et al., 1998; White and McKenzie, 1989).

On the other hand, the EM1-like Sr-Nd isotope signature in basalts may be of several different origins. For oceanic-island basalts, such a feature was interpreted as a mixture between HIMU OIB source and subducted pelagic sediments (Weaver, 1991; Hoffman, 1997). The EM1 isotopic signature in continental basalts has usually been considered either

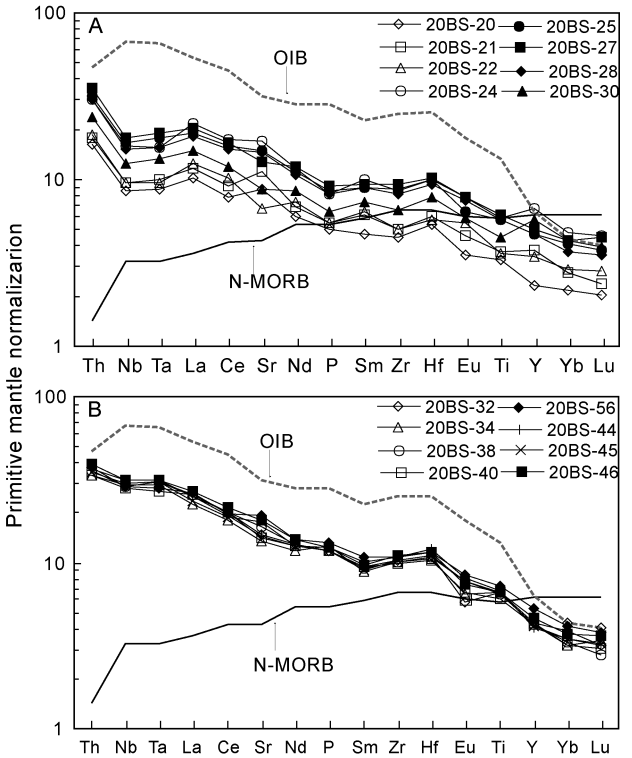

FIG. 5. Primitive mantle–normalized multi-element spidergrams of Upper Paleozoic basalts in the Youjiang Basin. Data sources: primitive mantle, N-MORB, and OIB are from Sun and McDonough (1989).

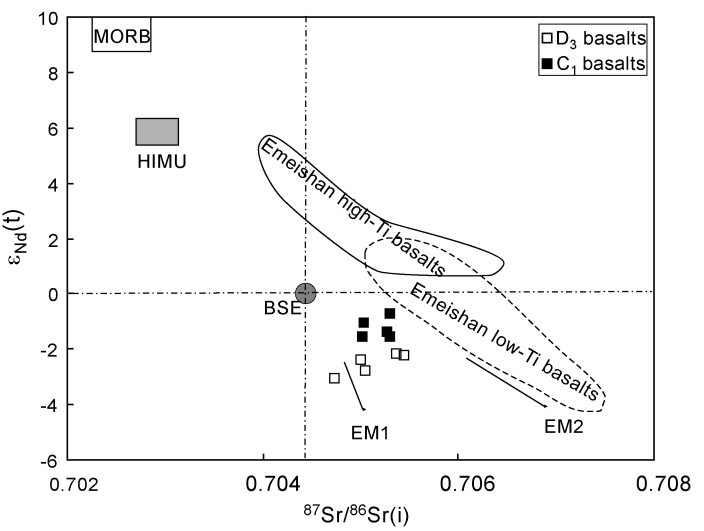

FIG. 6. Initial $^{87}Sr/^{86}Sr(i)$ vs. $\varepsilon_{Nd}(t)$ diagram of Upper Paleozoic basalts in the Youjiang Basin. Both basaltic suites show an EM1-type Sr-Nd isotopic signature. Isotope data of low-Ti and high-Ti basalts of Emeishan are from Xu et al. (2001) and Chung and Jahn (1995). The variation trends of EM1 and EM2, and fields of MORB and HIMU are from Hart (1988).

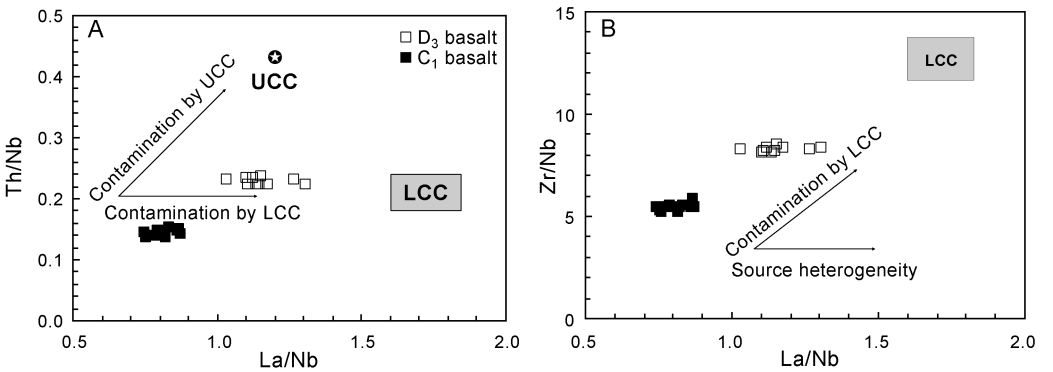

FIG. 7. La/Nb vs. Th/Nb (A) and Zr/Nb (B) plots of Upper Paleozoic basalts in the Youjiang Basin. Note that the slightly varying Th/Nb and Zr/Nb ratios follow La/Nb shifts in both basaltic suites, and favor heterogeneous sources instead of significant crust contamination during magma evolution.

as a feature inherited from enriched continental lithospheric mantle (CLM) (e.g., Menzies et al., 1987; Basu et al., 1991; Zhang et al., 1995), or as a mixture between an enriched SCLM and convective asthenosphere under an extensional regime (Jung and Hoernes, 2000; Gorring et al., 2003).

The high La/Nb, Th/Nb, and Zr/Nb in the tholeiites relative to average OIB suggest the importance of an enriched CLM in the source region (Table 1), whereas strong OIB-type trace element geochemistry (low La/Nb, Zr/Nb and Th/Nb) in the alkali basalts necessitates an important contribution by a depleted asthenosphere. Such geochemical and isotopic variation trends are well reflected in the La/Nb vs. $\varepsilon_{Nd}(t)$ diagram (Fig. 8), in which decreasing La/Nb is coupled with increasing $\varepsilon_{Nd}(t)$ grading from D_3 to C_1 basalts. Both basaltic suites were probably derived from heterogeneous mantle sources by two-component mixing between: (1) a low-La/Nb and high-$\varepsilon_{Nd}(t)$ component; and (2) a high-La/Nb and low-$\varepsilon_{Nd}(t)$ endmember. The fact that the alkali basalts have much lower La/Nb (0.74–0.87) and Zr/Nb (5.3–5.9) ratios than that of N-MORB (e.g., La/Nb = 1.07, Zr/Nb = 30; Sun and McDonough, 1989) indicates an OIB-type asthenosphere instead of an N-MORB-type one beneath the southern Yangtze block. In contrast, the high La/Nb and low $\varepsilon_{Nd}(t)$ endmember was probably an EM1-like lithospheric mantle that experienced moderate LILE and LREE enrichment prior to magma generation.

The major tectonic events that have likely affected the geochemical and isotopic evolution of the southern Yangtze CLM since stabilization beneath the continent include the following: (1) the break-up of the Rodinia supercontinent initially induced by a mantle plume at ~820 Ma (Li et al., 1999; Li and Powell, 2001; Li et al., 2002); (2) the closure of the Nanhua rift by the end of the Early Paleozoic (Cheng, 1994; Gilder et al., 1996); and (3) the opening of the Paleo-Tethyan Ocean beginning in at least Middle Devonian time (Zhang et al., 1985; Jian et al., 1998). Perhaps continuous metasomatism by small-fraction melts from MORB-like asthenosphere, coupled with periodic pulses of OIB-type melts during the breakup of Rodinia and the opening of the Paleo-Tethyan Ocean, could have produced the EM1-like isotopic signatures in the CLM beneath the southern Yangtze block.

Progressive rifting in the southern Yangtze block and its relationship with the Paleo-Tethyan Ocean

Lithospheric extension is usually considered as one of the most important causes for basaltic generation in continental settings (e.g., McKenzie and Bickle, 1988; White and McKenzie, 1989; Ellam, 1992; Chung et al., 1994; Polat et al., 1997). In such cases, asthenospheric upwelling and thermomechanical erosion of the basal lithosphere mantle lead to significant lithospheric thinning and decompression melting, once the geotherm encounters the peridotite solidus (e.g., McKenzie and Bickle, 1988; Hirose and Kushiro, 1993).

Compared with the overlying enriched CLM beneath the southern Yangtze block, the underlying asthenosphere must have relatively lower LREE/MREE values. Accordingly, the increasing La/Sm and ε_{Nd} values coupled with decreasing La/Nb from the tholeiites to the alkali basalts (Figs. 8 and 9)

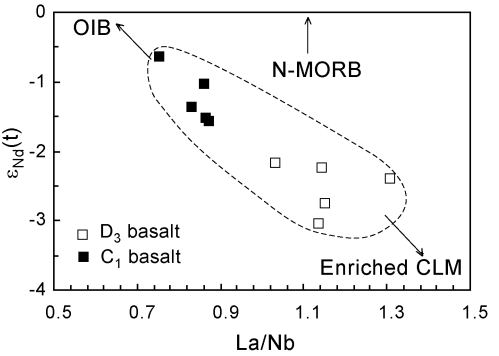

FIG. 8. La/Nb vs. $\varepsilon_{Nd}(t)$ diagram of Upper Paleozoic basalts in the Youjiang Basin, showing a two-component mixing trend between an OIB-type asthenosphere and an enriched CLM beneath the southern Yangtze block.

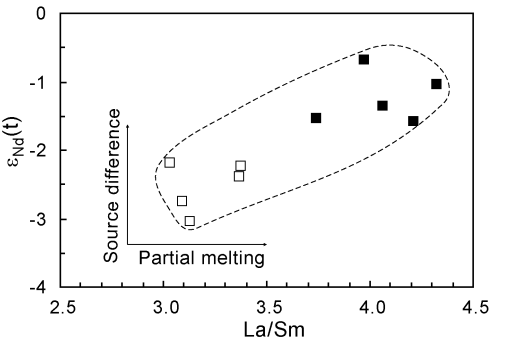

Fig. 9. La/Sm vs. $\varepsilon_{Nd}(t)$ plots of Upper Paleozoic basalts in the Youjiang Basin.

tend to indicate that the D_3 tholeiites were produced through larger degrees of melting of a mixed source with higher proportions of enriched CLM, whereas the C_1 alkali basalts were generated by smaller degrees of melting of a mixture with less enriched components. Such trends grading from D_3 to C_1 basalts reflect thermo-mechanical erosion of the lithospheric mantle by underlying asthenosphere, and progressive rifting episodes in the southern Yangtze block.

Furthermore, the distinguishable trace-element geochemistry of the Upper Paleozoic Youjiang Basin basalts from island-arc volcanics precludes the existence of contemporaneous subducted slabs underneath the southern Yangtze block. In combination with an intracontinental rifting model for basalt generation, it is reasonable to conclude that the southern Yangtze block became a passive continental margin during Late Paleozoic time, following the opening and spreading of the Paleo-Tethyan Ocean.

It is still unclear when the paleo-Tethyan Ocean began to open, but the occurrence of MORB-like gabbros of 385–340 Ma from Tongchangjie and Shuanggou ophiolite suites in Yunan province along the Honghe-Ailaoshan fault suggest that oceanic basaltic crust existed at least since the Middle Devonian (Zhang et al., 1985, 1988; Jian et al., 1998). Following oceanic opening and spreading, upwelling of convective asthenosphere triggered passive continental rifting and crustal stretching along the southern Yangtze block, and the formation of the primal Youjiang Basin (Chen et al., 1994, 2000; Cheng, 1994; Qin et al., 2000).

Conclusions

Upper Paleozoic basaltic lavas extruded in the Youjiang Basin from the southern Yangtze block are compositionally heterogeneous, grading from D_3 tholeiitic to C_1 alkali basalts. These rocks show variably enriched in incompatible elements (LREE, Th, Zr, Hf) and EM1-like Sr-Nd isotopic compositions. Such features were inherited from a mixed source between an OIB-type asthenosphere and an EM1-like CLM. Compared with alkali basalts, tholeiites that have lower abundances of incompatible elements but higher La/Nb, Th/Nb, and Zr/Nb ratios were produced through higher-degree melting of the mixed source with an important contribution of the enriched components; in contrast, alkali basalts were generated by lower-degree melting of the mixed source with a lower proportion of the enriched components. The petrogenesis of Upper Paleozoic basalts in the southern Yangtze block favored a progressive rifting model as a consequence of lithosphere-asthenosphere interaction, suggesting that it became a passive continental margin following the opening and spreading of Paleo-Tethys.

Acknowledgments

The authors thank Prof. R. F. Zhang for his assistance in Sr and Nd isotope analysis, and Mr. L. Qi for his help in the ICP-MS analysis. This study was financially supported by the National Ministry of Science and Technology of China (No. G1999043205) and the Chinese Academy of Sciences (KXCX2-101).

REFERENCES

Arculus, R. J., 1994, Aspects of magma genesis in arcs: Lithos, v. 33, p. 189–208.

Basu, A. R., Wang, J., Huang, W., Xie, G., and Tatsumoto, M., 1991, Major element, REE, and Pb, Nd, and Sr isotopic chemistry of Cenozoic volcanic rocks of eastern China: Implications for their origin from suboceanic-type mantle reservoirs: Earth and Planetary Science Letters, v. 105, p. 149–169.

Chen, H. D., Qin, J. X., Tian, J. C., Peng, J., and Hou, Z. J., 2000, Sequence filling dynamics of the Youjiang basin, southern China: Acta Sedimentologica Sinica, v. 18, p. 165–171 (in Chinese with English abstract).

Chen, H. D., Zhang, J. Q., and Liu, W. J., 1994, Structure of Youjiang basin in the Devonian–Carboniferous period and its evolution of lithofacies and paleogeography: Guangxi Geology, v. 7, p. 15–23 (in Chinese).

Cheng, Y. Q., 1994, An outline of regional geology in China: Beijing, China, Geological Publishing House, 517 p. (in Chinese).

Chung, S. L., Sun, S. S., Tu, K., Chen, C. H., and Lee, C. Y., 1994, Late Cenozoic basaltic volcanism around the Taiwan Strait, SE China: Product of lithosphere-asthenosphere interaction during continental extension: Chemical Geology, v. 112, p. 1–20.

Chung, S. L., and Jahn, B. M., 1995, Plume-lithosphere interaction in generation of the Emeishan flood basalts at the Permian–Triassic boundary: Geology, v. 23, p. 889–892.

Davies, J. H., and Stevenson, D. J., 1992, Physical model of source region of subduction zone volcanics: Journal of Geophysical Research, v. 97, p. 2037–2070.

Ellam, R. M., 1992, Lithospheric thickness as a control on basalt geochemistry: Geology, v. 20, p. 153–156.

Floyd, P. A., and Winchester, J. A., 1978, Identification and discrimination of altered and metamorphosed volcanic rocks using immobile elements: Chemical Geology, v. 21, p. 291–306.

Gilder, S. A., Gill, J., Coe, R. S., Zhao, X. X., Liu, Z. W., and Wang, G. X., 1996, Isotopic and paleomagnetic constraints on the Mesozoic tectonic evolution of South China: Journal of Geophysical Research, v. 107, p. 16,137–16,154.

Gorring, M., Singer, B., Jason, G., and Kay, S. M., 2003, Plio-Pleistocene basalts from the Meseta del Lago Buenos Aires, Argentina: Evidence for asthenosphere-lithosphere interactions during slab window magmatism: Chemical Geology, v. 193, p. 215–235.

Griffiths, R. W., and Campbell, I.H., 1991, Interaction of mantle plume heads with the Earth's surface and onset of small-scale convection: Journal of Geophysical Research, v. 96, p. 18295–18310.

Grove, T. L., and Kinzler, R. J., 1986, Petrogenesis of andesites: Annual Review of Earth and Planetary Science, v. 14, p. 417–454.

GXBGMR (Guangxi Bureau of Geology and Mineral Resources), 1985, Regional geology of Guangxi Province: Beijing, China, Geological Publishing House, 853 p. (in Chinese).

Hart, S. R., 1988, Heterogeneous mantle domains: Signature, genesis, and mixing chronologies: Earth and Planetary Science Letters, v. 90, p. 273–296.

Hirose, K., and Kushiro, I., 1993, Partial melting of dry peridotites at high pressures: Determination of compositions of melts segregated from peridotite using aggregates of diamond: Earth and Planetary Science Letters, v. 114, p. 477–489.

Hoffman, A. W., 1997, Mantle geochemistry: The message from oceanic volcanism: Nature, v. 385, p. 219–229.

Hunter, A. G., and Blake, S., 1995, Petrogenetic evolution of a transitional tholeiitic–calc-alkaline series: Towada volcano, Japan: Journal of Petrology, v. 36, p. 1579–1605.

Jian, P., Wang, X. F., He, L. Q., and Wang, C. S., 1998, U-Pb zircon dating of the Shuanggou ophiolite from Xingping County, Yunnan Province: Acta Petrologica Sinica, v. 14, p. 207–211 (in Chinese with English abstract).

Jung, S., and Hoernes, S., 2000, The major- and trace-element and isotope (Sr, Nd, O) geochemistry of Cenozoic alkaline volcanic rocks from the Rhön area (Central Germany): Petrology, mantle source characteristics, and implications for asthenosphere-lithosphere interactions: Journal of Volcanology and Geothermal Research, v. 99, p. 27–53.

Lafléche, M. R., Camiré, G., and Jenner, G. A., 1998, Geochemistry of post-Acadian, Carboniferous continental intraplate basalts from the Maritimes Basin, Magdalen Islands, Quebéc, Canada: Chemical Geology, v. 148, p. 115–136.

Li, X. H., 1999, Geochemical constraints on the Proterozoic crustal growth and evolution: A case study of the South China Block, *in* Zheng, Y. F., ed., Chemical geodynamics: Beijing, China: Science Press, p. 288–316 (in Chinese).

Li, X. H., Li, Z. X., Zhou, H. W., Liu, Y., and Kinny, P. D., 2002, U-Pb zircon geochronology, geochemistry, and Nd isotopic study of Neoproterozoic bimodal volcanic rocks in the Kangdian Rift of South China: Implications for the initial rifting of Rodinia: Precambrian Research, v. 113, p. 135–154.

Li, Z. X., Li, X. H., Kinny, P. D., and Wang, J., 1999, The breakup of Rodinia: Did it start with a mantle plume beneath South China?: Earth and Planetary Science Letters, v. 173, p. 171–181.

Li, Z. X., and Powell, C. McA., 2001, An outline of the paleogeographic evolution of the Australian region since the beginning of the Neoproterozoic: Earth Science Review, v. 53, p. 237–277.

Li, Z. X., Zhang, L., and Powell, C. McA., 1995, South China in Rodinia: Part of the missing link between

Australia–East Antarctica and Laurentia?: Geology, v. 23, p. 407–410.

McKenzie, D. P., and Bickle, M. J., 1988, The volume and composition of melt generated by extension of the lithosphere: Journal of Petrology, v. 29, p. 625–679.

Menzies, M. A., Rogers, N., Tindle, A., and Hawkesworth, C. J., 1987, Metasomatic and enrichment processes in lithospheric peridotites, an effect of asthenosphere-lithosphere interaction, *in* Menzies, M. A., and Hawkesworth, C. J., eds., Mantle metasomatism: London, UK, Academic Press, p. 313–361.

Peng, Z. X., Mahoney, J., Hooper, P., Harris, C., and Beane, J., 1994, A role for lower continental crust in flood basalt genesis? Isotopic and incompatible element study of the lower six formations in the western Deccan Traps: Geochimica et Cosmochimica Acta, v. 58, p. 255–269.

Polat, A., Kerrich, R., and Casey, J. F., 1997, Geochemistry of Quaternary basalts erupted along the east Anatolian and Dead Sea fault zones of southern Turkey: Implications for mantle source: Lithos, v. 40, p. 55–68.

Qi, L., Hu, J., and Grégoire, D. C., 2000, Determination of trace elements in granites by inductively coupled plasma mass spectrometry: Talanta, v. 51, p. 507–513.

Qin, J. X., Chen, H. D., Tian, J. C., and Yang, Z. S., 2000, Sequence filling succession and paleo-Tethyan Sea reconstruction of the Youjiang basin, southern China: Acta Geoscientia Sinica, v. 21, p. 62–70 (in Chinese with English abstract).

Ren, J. X., Wang, Z. X., Chen, B. W., Jiang, C. F., Niu, B. G., Li, J. Y., Xie, G. L., He, Z. J., and Liu, Z. G., 1999, The tectonics of China from a global view: A guide to the tectonic map of China and adjacent regions: Beijing, China, Geological Publishing House, 32 p.

Rudnick, R. L., and Fountain, D. M., 1995, Nature and composition of the continental crust: A lower crustal perspective: Reviews of Geophysics, v. 33, p. 267–309.

Smedley, P. L., 1986, The relationship between calc-alkaline volcanism and within-plate continental rift volcanism: Evidence from Scottish Palaeozoic lavas: Earth and Planetary Science Letters, v. 76, p. 113–128.

Sun, S. S., and McDonough, W. F., 1989, Chemical and isotopic systematics of oceanic basalts: Implication for mantle composition and processes, *in* Saunder, A. D., and Norry, M. J., eds., Magmatism in the ocean basins: Geological Society of London Special Publication, v. 42, p. 313–345.

Taylor, S. R., and McLennan, S. M., 1985, The continental crust: Its composition and evolution: Oxford UK, Blackwell, 312 p.

Wang, Z. C., Wu, H. R., and Kuang, G. D., 1997, Characteristics of the late Paleozoic basalts and their eruptive environments in western Guangxi: Acta Petrologica Sinica, v. 13, p. 260–265 (in Chinese with English abstract).

Weaver, B. L., The origin of ocean-island basalts end-member composition: Trace element and isotopic constraints: Earth and Planetary Science Letters, v. 104, p. 381–397.

White, R., and McKenzie, D. P., 1989, Magmatism at rift zones: The generation of volcanic continental margins and flood basalts: Journal of Geophysical Research, v. 94, p. 7685–7729.

Xu, Y. G., Chung, S. L., Jahn, B. M., and Wu, G. Y., 2001, Petrological and geochemical constraints on the petrogenesis of Permian–Triassic Emeishan flood basalts in southwestern China: Lithos, v. 58, p. 145–168.

Zhang, M., Suddaby, P., Thompson, R. N., Thirlwall, M. F., and Menzies, M. A., 1995, Potassic volcanic rocks in NE China: Geochemical constraints on mantle source and magma genesis: Journal of Petrology, v. 36, p. 1275–1303.

Zhang, Q., Li, D. Z., Zhang, K. W., 1985, A preliminary study on the ophiolitic nappes from Tongchangjie, Yunnan Province: Acta Petrologica Sinica, v. 1, no. 3, p. 1–4 (in Chinese).

Zhang, Q., Zhang, K. W., Li, D. Z., and Wu, H. W., 1988, A preliminary study on Shuanggou ophiolite suite from Pingxian County, Yunnan Province: Acta Petrologica Sinica, v. 4, no. 3, p. 37–48 (in Chinese).